Published in final edited form as:
Science. 2017 February 10; 355(6325): 641–647. doi:10.1126/science.aal3908.

A switch from canonical to noncanonical autophagy shapes B cell responses

Nuria Martinez-Martin[#1,*], **Paula Maldonado**[#1], **Francesca Gasparrini**[1], **Bruno Frederico**[1], **Shweta Aggarwal**[1], **Mauro Gaya**[1,4], **Carlson Tsui**[1], **Marianne Burbage**[1], **Selina Jessica Keppler**[1], **Beatriz Montaner**[1], **Harold B.J. Jefferies**[3], **Usha Nair**[4], **Yan G. Zhao**[5], **Marie-Charlotte Domart**[2], **Lucy Collinson**[2], **Andreas Bruckbauer**[1,6], **Sharon A. Tooze**[3,*], and **Facundo D. Batista**[1,4,*]

[1]Lymphocyte Biology Laboratory, Francis Crick Institute, 1 Midland Road, London NW1 1AT, UK

[2]Electron Microscopy Unit, Francis Crick Institute, 1 Midland Road, London NW1 1AT, UK

[3]Molecular Cell Biology of Autophagy Laboratory, Francis Crick Institute, 1 Midland Road, London NW1 1AT, UK

[5]Institute of Biophysics, Chinese Academy of Sciences, 15 Datun Road, Chaoyang District, Beijing 100101, China

[6]FILM facility, Imperial College London, Exhibition Road, London, SW7 2AZ, UK

[#] These authors contributed equally to this work.

Abstract

Autophagy is important in a variety of cellular and pathophysiological situations; however, its role in immune responses remains elusive. Here, we show that among B cells, germinal center (GC) cells exhibited the highest rate of autophagy during viral infection. In contrast to mechanistic target of rapamycin complex 1-dependent canonical autophagy, GC B cell autophagy occurred predominantly through a noncanonical pathway. B cell stimulation was sufficient to down-regulate canonical autophagy transiently while triggering noncanonical autophagy. Genetic ablation of WD repeat domain, phosphoinositide-interacting protein 2 in B cells alone enhanced this noncanonical autophagy, resulting in changes of mitochondrial homeostasis and alterations in GC and antibody secreting cells. Thus, B cell activation prompts a temporal switch from canonical to noncanonical autophagy that is important in controlling B cell differentiation and fate.

Macroautophagy (hereafter called autophagy) is a conserved, lysosomal pathway that degrades cytosolic content and provides a means for cellular survival during stressful conditions. Autophagy is involved in several areas of the immune response (1, 2). In B cells, autophagy has been described as an essential process for the maintenance of plasma cell (PCs) and survival of memory B cell (3–5). However, given the high and stressful energy

[*]Authors to whom correspondence should be addressed: fbatista1@mgh.harvard.edu, nuria.martinezmartin@crick.ac.uk, sharon.tooze@crick.ac.uk.
[4]Ragon Institute of MGH, MIT and Harvard, Cambridge, Massachusetts 02139, USA.

Europe PMC Funders Author Manuscripts

demand that B cells require following activation, we investigated the role of autophagy in the early steps of B cell activation following viral infection.

Autophagosome formation requires the localization of phosphatidylethanolamine conjugated LC3 (LC3-II) to the autophagosome membrane (6, 7). Accordingly, LC3-II accumulation was used to examine the role of autophagy in vivo during the course of an immune response. Transgenic mice expressing LC3 fused to a green fluorescent protein (GFP-LC3) were infected with Murid Herpesvirus-4 (MuHV-4) and spleen sections were examined. Germinal center (GC) B cells characterized by $Bcl6^{high}IgD^{low}$ staining, exhibited higher levels of GFP-LC3 staining compared with $Bcl6^{low}IgD^{high}$ mantle cells (surround GC) (Fig. 1A). Similar results were observed after the addition of chloroquine, an inhibitor that prevents the lysosomal breakdown of autophagosomes, compared with antibody-secreting cells (ASCs) (Fig. S1A and S1B). Flow cytometry analysis also revealed that GC B cells had a greater than two-times increase in vesicular GFP-LC3-II compared with follicular B cells (Fig. 1B).

Next, we examined the autophagic flux in B cells by visualizing the accumulation of GFP-LC3-II using two commonly used autophagy inhibitors, bafilomycin A1 (BafA1) or chloroquine, which block LC3-II degradation differently (8). Whereas a comparable block in autophagy flux was observed in the different B cell types (follicular, GCs, ASC, and memory) after treatment with BafA1 (Fig. 1C), a significantly increased flux was observed only in GC B cells in response to chloroquine (Fig. 1C and 1D, and Fig. S1C, D, E and F). This increased LC3-II flux in GC B cells was recapitulated in chloroquine-treated spleen tissue (Figure S1A).

The results from flow cytometry analyses were quantitated using an autophagy index (AI), wherein we defined total autophagy flux as the mean fluorescence intensity (MFI) after chloroquine treatment, canonical autophagy flux as the MFI after Baf A1 treatment, and the noncanonical autophagy flux as the difference between the two normalized by the MFI of LC3-II before inhibitor addition (Fig. 1C and Fig. S1D). When GCs cells were sub-divided into centrocytes (light zone) and centroblasts (dark zone), both cell populations showed an elevated noncanonical autophagy flux, with centrocytes exhibiting a reduction in canonical autophagy flux compared to centroblasts (Fig. 1E and Fig. S1G and H). Thus, GC B cells not only have the highest LC3-II levels but also exhibit an atypical flux.

B cell receptor (BCR) stimulation of naïve follicular cells was sufficient to inhibit the canonical accumulation of LC3-II while at the same time triggering the increase of noncanonical accumulation of LC3-II (Fig. 1F and S2A, B, and C). Consistent with a diminution in canonical autophagy, levels of p62 (a receptor protein for cargo degraded via autophagy) increased (Fig. S2D), indicating that upon activation B cells switch from canonical to noncanonical accumulation of LC3-II. In vitro, the levels of canonical autophagy were restored 1 day after stimulation (Fig. 1G and Fig. S3A); however, total autophagy peaked 2 days following stimulation At this point, LC3-II could be detected by immunoblot even in the absence of any inhibitor (Fig. S3B). Furthermore, a similar switch in autophagy was apparent when B cells were activated by other means such as CD40 stimulation (Fig. S2A, B and C).

Canonical autophagy is triggered by the inactivation of mechanistic target of rapamycin complex 1 (mTORC1) (9). However, in activated B cells, the mTORC1 substrate, phosphorylated ribosomal protein S6 kinase (p-pS6K), was significantly elevated (10, 11)) [10-fold upon BCR cross-linking (Fig. 2A) and at least 2-fold in GC B cells (Fig. 2B)]. This mTORC1 activity decreased after 20 hours of stimulation, consistent with a restoration of the levels of canonical autophagy (Fig. 1G, 2A and Fig. S3A). Furthermore, this atypical autophagy flux was dependent on SYK, PLCγ2, BLNK, VAV, and PI3K activity, but apparently not on class III PI3K required for canonical autophagy (12, 13) (Fig. 2C, D and Fig. S4A, B and C). Thus, the noncanonical accumulation of LC3-II in activated B cells might become physiologically relevant when the levels of mTORC1 are high.

We next followed the intracellular recruitment of four components of the autophagy machinery -ATG9L1, ATG16L1, WD repeat domain, phosphoinositide-interacting protein 2 (WIPI2), and LC3 (14)- in A20 B cells following BCR stimulation in real-time using total internal reflection fluorescence (TIRF) microscopy. While we observed some colocalization of the early autophagy marker ATG9 to antigen clusters (Fig. 2E and Movie S1), we were unable to detect any recruitment of WIPI2, ATG16L1 and LC3, suggesting that these proteins might be recruited later during antigen internalization (Fig. S5A, B and C and Movie S2, 3, 4). To analyze this further, we used structured illumination microscopy (SIM) to localize WIPI2 and Atg16L1 in wild-type (WT) primary naïve B cells following BCR stimulation. Fifteen minutes after BCR stimulation, the internalized antigen was present in ring-like structures decorated with WIPI2 or Atg16L1 (Fig. 2F and Movie S5, S6 and S7). A closer analysis of the antigen containing ring-like structures using a combination of correlative SIM and transmission electron microscopy (TEM) suggested that the antigen-containing ringlike structures might be constituted predominantly of a single membrane (Fig. 2G and Movie S7). These results indicate an early recruitment of the autophagy membrane during B cell activation as well as an accumulation of autophagy proteins to unusual ringlike structures, which surround the internalized antigen.

Given the colocalization of antigen with WIPI2 and ATG16L1, we wanted to elucidate the role of this pathway in B cell activation following a genetic approach. We conditionally deleted ATG16L1 in B cells by crossing ATG16L1$^{flox/flox}$ mice with mice expressing cre recombinase from either MB1 or Cd19 promoters. With the exception of a reduction of B1a cells in the peritoneal cavity, ATG16L1 knockout (KO) B cells developed normally and were phenotypically indistinguishable from those of their WT littermates (Fig. S6 and S7). Our attempts to conditionally ablate WIPI2 in the B cell compartment resulted in mice expressing low amounts of an aberrant version of WIPI2 (WIPI2-KO^{p}) (Fig. S8A and C). Therefore, we developed a second WIPI2-KO line of mice using the CRISPR (clustered regularly interspaced short palindromic repeats)-Cas9 technology, which led to complete WIPI2 deletion (Fig S8B and C). In order to study the function of WIPI2 in B cells, we took advantage of WIPI2-KO ^{p} bone marrow (BM), or WIPI2-KO fetal liver (FL) to generate mixed chimeras (Materials and Methods). In both WIPI2-KO and WIPI2-KO^{p} mice, B cells developed and differentiated normally giving rise to normal numbers of B cells in the spleen, but they lacked the B1 compartment (Fig. S9 and S10).

Upon antigen challenge, the WIPI2-KO and WIPI2-KO^{P} chimeras showed a significant reduction in GC B cells and a diminution of centroblasts during B cell immune response (Fig. 3A, B and Fig. S11C and G). Whereas the percentage of ASCs was substantially reduced in the WIPI2-KO mice, there was an increase of these cells in the WIPI2-KO^{P} mice (Fig. 3B). Consistent with these results, we observed enhanced levels of immunoglobulin M (IgM) but decreased immunoglobulin G (IgG) in WIPI2-KO^{P} mice and reduced frequency of IgG-producing cells using an enzyme-linked immunospot (ELISPOT) assay (Fig. S11D and E). Finally, we found statistically insignificant reduction of memory cells in WIPI2-KO (Fig. S11F). However, ATG16L1-KO mice did not exhibit such marked immune alterations when compared to their WT littermates (Fig. 3A and B, and Fig. S11A and B). Thus, GC B cell formation and ASC differentiation require WIPI2 and, to a lesser degree, ATG16L1.

To study the effect of WIPI2 and ATG16L1 deletion on B cell autophagy, LC3-II accumulation was examined in naïve, stimulated B cells and GC B cells in the presence and absence of chloroquine and Baf A1 with flow cytometry. As expected, ablation of ATG16L1 led to a complete absence of LC3-II under all treatment conditions (Fig. 3C and D and Fig. S13A). Surprisingly, WIPI2-deficient naïve B cells exhibited elevated levels of LC3-II even in the absence of stimulation or the presence of any inhibitor (Fig. 3C and Fig. S12A). Furthermore, compared to WT B cells, both resting and BCR-stimulated WIPI2-KO B cells exhibited a twofold higher LC3-II accumulation after chloroquine but not Baf A1 treatment (Fig. 3C and D; Fig. S12A and B. S13B), indicating that these B cells lack canonical autophagy while having enhanced noncanonical LC3-II accumulation. Similar results were obtained in naïve B cells lacking ULK1/ULK2 or when Beclin-1 or WIPI-2 were genetically ablated in B cells lines, adding to the notion that this is the result of noncanonical accumulation of LC3 (Fig S12C-F). Additionally, the accumulation of p62 in WIPI2-KO cells is indicative of the lack of canonical autophagy, which was also what we observed in ATG16L1-KO cells (Fig. S12G). Consistent with the notion of a key role for WIPI2 in the GC, the expression of this protein was enhanced 10-fold in GCs compared to other B cell types (Fig. S12H). Thus, whereas canonical autophagy is abolished in ATG16L1- and WIPI2-deficient B cells, WIPI2-KO cells exhibit a higher noncanonical accumulation of LC3-II.

We then determined the effect that WIPI2 and ATG16L1 ablation on B cell proliferation and differentiation in vitro. We tracked B cell division and ASC differentiation according to the dilution of CTV (CellTrace Violet dye) and the appearance CD138^{+} cells, respectively; in CpG-stimulated B cells isolated from WIPI2-KO, Atg16L1-KO or WT mice. Whereas the proliferation of both ATG16L1-KO and WIPI2-KO B cells was comparable to that of WT, the number of ASCs was significantly higher in WIPI2-KO cells (Fig. 4A and Fig. S14A). Compared to WT cells, which require at least three divisions to acquire ASC markers, WIPI2-KO B cells needed only two cell divisions (Fig. 4A and Fig. S14A). Similar results were obtained when B cells were treated with resveratrol, an agent known to induce Beclin-1-independent noncanonical autophagy (Fig. S15A and B) (9). Thus, the absence of WIPI2, but not ATG16L1, is sufficient to enhance differentiation to ASC in vitro, likely owing to their higher levels of noncanonical LC3 accumulation in WIPI2-KO cells.

Upon antigenic challenge, both WIPI2- and ATG16L1-deficient cells were capable of forming antigen-containing ring structures; however, unlike B cells lacking ATG16L1, WIPI2-deficient B cells had more antigen-containing ringlike structures compared to WT after 15 minutes or after 5 hours BCR stimulation in the presence of chloroquine (Fig. 4B, Fig. S16A and B and Movie S8). Thus, the absence of WIPI2, but not ATG16L1, might cause cellular alterations affecting antigen internalization. Intriguingly, correlative SIM and TEM showed mitochondrial fragments that appear to be surrounded, or even engulfed, by these rings (Fig. 4C and Movie S9).

Mitochondrial status has been suggested as a signal for initiating B cell differentiation (15). Although no mitochondrial alterations were observed in Atg16L1-KO naïve resting B cells when compared to WT, WIPI2-KO naïve resting B cells exhibited higher levels of reactive oxygen species (ROS), mitochondrial mass (MM) and mitochondrial membrane potential (MMP) than WT cells (Fig. 4D and Fig. S14B). Additionally, both the basal oxygen consumption rate (OCR), and the basal extracellular acidification rate (ECAR) were significantly higher in WIPI2-KO B cells (Fig. 4E). Furthermore, phosphoS65-parkin, a key mitochondrial degradation protein involved in ubiquitin-dependent degradation and mitophagy, was increased at steady state but not following BCR stimulation in WIPI2-KO B cells (Fig. 4F). Furthermore, following CpG stimulation, a low-MM and low-MMP mitochondrial population appeared more rapidly in WIPI2-KO cells compared to WT cells (Fig. 4G and Fig. S14C). This is consistent with the higher numbers of ASC observed in the cultures (Fig. 4A and Fig. S14A). Similar results were also obtained when WT B cells treated with resveratrol, (Fig. S15C). These results highlight a role for WIPI2 in mitochondrial homeostasis during B cell activation and cell differentiation.

During adaptive immune responses, B cell activation results in a highly proliferative stage, where B cells expand and differentiate either outside the follicles into short-lived PCs and early recirculating memory B cells or they enter into the GCs. In the GCs, B cell proliferation and differentiation results in the formation of long-lived PCs and memory B cells with improved affinity for the antigen. This stage is intricately linked with a switch in the metabolic program of cells toward providing building blocks for the synthesis of various biomolecules and meeting the energetic demands at the cellular level (16). Autophagy enables recycling of macromolecules that serve as a source of building blocks and energy required for cell survival under stress. Considering this high demand for energy and resources during the differentiation of follicular B cells into GCs, it is somewhat surprising that, until now, autophagy has been described to be essential only in memory and PC survival (4, 5). Our data highlights the importance of autophagic processes during the B cell immune response.

Overall, we have established that GC B cells exhibit increased basal levels of noncanonical LC3 accumulation, which is recapitulated when naïve B cells are activated. This increased accumulation of LC3 appears to occur through predominantly noncanonical pathways and is driven by a temporary switch that down-regulates from canonical autophagy. This switch, initiated during B cell activation, might be of importance at the centrocyte stage, where GCs cells are exposed to antigen stimulation and T cell help in vivo. Antigen stimulation of the B cells through BCR or T cell help increases mTOR activity (10, 11), which in turn will down-

Europe PMC Funders Author Manuscripts

regulate canonical autophagy while inducing the noncanonical accumulation of LC3-II. These autophagy alterations might associate with endosomal regulation to allow T cell presentation as well as changes in mitochondrial homeostasis to help B cells to divide.

The absence of WIPI2, but not ATG16L1, promoted an imbalance in the amount of LC3-II and the nature of autophagy in B cells. This resulted in a lack of canonical autophagy and an increase in noncanonical accumulation of LC3-II within WIPI2-KO B cells. These changes were associated with alterations in the mitochondrial status and the metabolic profile of B cells, which affects GC reaction and ASC differentiation. We propose that WIPI2 is an important regulator of autophagy and mitochondria homeostasis in B cells and thus influences B cell differentiation and fate.

Supplementary Material

Refer to Web version on PubMed Central for supplementary material.

Acknowledgements

We thank the flow cytometry and biological resource units at the Francis Crick Institute for their help. We are grateful to P. Stevenson (University of Queensland, Brisbane, Australia) for the MuHV4 mice; H. W. Virgin (Washington University School of Medicine) and K. Maloy (Sir William Dunn School of Pathology, University of Oxford) for kindly providing the Atg16L1 floxed mice. M. Reth (Max Planck Institute, Freiburg, Germany) for the Mb1-Cre mice. H. Zhang (Institute of Biophysics, Chinese Academy of Sciences, Beijing, China) for providing WIPI2-KO mice; and K. Okkenhaug, (Babraham Institute, Cambridge, UK) for Vps34 IN1. We thank all members of the Lymphocyte Biology Laboratory for support and critical discussion. This work was supported by the Francis Crick Institute, which receives its core funding from Cancer Research UK (FC001035, FC001187, FC001136), the UK Medical Research Council (FC001035, FC001187, FC001136), and the Wellcome Trust (FC001035, FC001187, FC001136). The Center for HIV/AIDS Vaccine Immunology and Immunogen Discovery of the National Institute of Health (UM1AI100663); the Phillip T. and Susan M. Ragon Institute Foundation; a Marie Sklodowska-Curie individual postdoctoral fellowship (N.MM), Abroad Doctoral Fellowships, Scholarships Chile granted by CONICYT (P.M), the Institute Pasteur-Fondazione Cenci Bolognetti (F.G), a long-term European Molecular Biology Organization (EMBO) fellowship (N.MM and S.A), and a German Research Foundation grant (S.J.K).

References

1. Shibutani ST, Saitoh T, Nowag H, Munz C, Yoshimori T. Nat Immunol. 2015; 16:1014. [PubMed: 26382870]
2. Levine B, Mizushima N, Virgin HW. Nature. 2011; 469:323. [PubMed: 21248839]
3. Arnold J, et al. Cell Death Differ. 2016; 23:853. [PubMed: 26586568]
4. Chen M, et al. Nat Med. 2014; 20:503. [PubMed: 24747745]
5. Pengo N, et al. Nat Immunol. 2013; 14:298. [PubMed: 23354484]
6. Kabeya Y, et al. EMBO J. 2000; 19:5720. [PubMed: 11060023]
7. Kabeya Y, et al. J Cell Sci. 2004; 117:2805. [PubMed: 15169837]
8. Florey O, Gammoh N, Kim SE, Jiang X, Overholtzer M. Autophagy. 2015; 11:88. [PubMed: 25484071]
9. Codogno P, Mehrpour M, Proikas-Cezanne T. Nat Rev Mol Cell Biol. 2012; 13:7.
10. Donahue AC, Fruman DA. Eur J Immunol. 2007; 37:2923. [PubMed: 17724683]
11. Limon JJ, Fruman DA. Front Immunol. 2012; 3:228. [PubMed: 22888331]
12. Petiot A, Ogier-Denis E, Blommaart EF, Meijer AJ, Codogno P. The Journal of biological chemistry. 2000; 275:992. [PubMed: 10625637]
13. Martinez J, et al. Nat Cell Biol. 2015; 17:893. [PubMed: 26098576]
14. Feng Y, He D, Yao Z, Klionsky DJ. Cell Res. 2014; 24:24. [PubMed: 24366339]
15. Jang KJ, et al. Nat Commun. 2015; 6:6750. [PubMed: 25857523]

16. Heise N, et al. J Exp Med. 2014; 211:2103. [PubMed: 25180063]
17. Conway, KL., et al. Gastroenterology. Vol. 145. Elsevier, Inc; 2013. p. 1347-1357.
18. Hobeika E, et al. Proceedings of the National Academy of Sciences. 2006; 103:13789.
19. Frederico, B., Chao, B., May, JS., Belz, GT., Stevenson, PG. Cell Host and Microbe. Vol. 15. Elsevier Inc; 2014. p. 457-470.
20. Cong L, et al. Science. 2013; 339:819. [PubMed: 23287718]
21. Ran FA, et al. Nat Protoc. 2013; 8:2281. [PubMed: 24157548]
22. Gustafsson MG, et al. Biophysical journal. 2008; 94:4957. [PubMed: 18326650]
23. Costes SV, et al. Biophysical journal. 2004; 86:3993. [PubMed: 15189895]
24. Manders EMM, Verbeek FJ, Aten JA. Journal of Microscopy. 1993; 169:375.
25. Schindelin J, et al. Nature methods. 2012; 9:676. [PubMed: 22743772]
26. Cardona A, et al. PloS one. 2012; 7:e38011. [PubMed: 22723842]
27. Eng KE, Panas MD, Hedestam GBK, McInerney GM. Autophagy. 2010; 6:634. [PubMed: 20458170]
28. de la Calle C, Joubert P-E, Law HKW, Hasan M, Albert ML. autophagy. 2011; 7:1045–1051. [PubMed: 21606680]
29. Phadwal K, et al. autophagy. 2012; 8:677–689. [PubMed: 22302009]

Europe PMC Funders Author Manuscripts

One Sentence Summary

Non-canonical autophagy, triggered after B cell activation, tunes B cell responses.

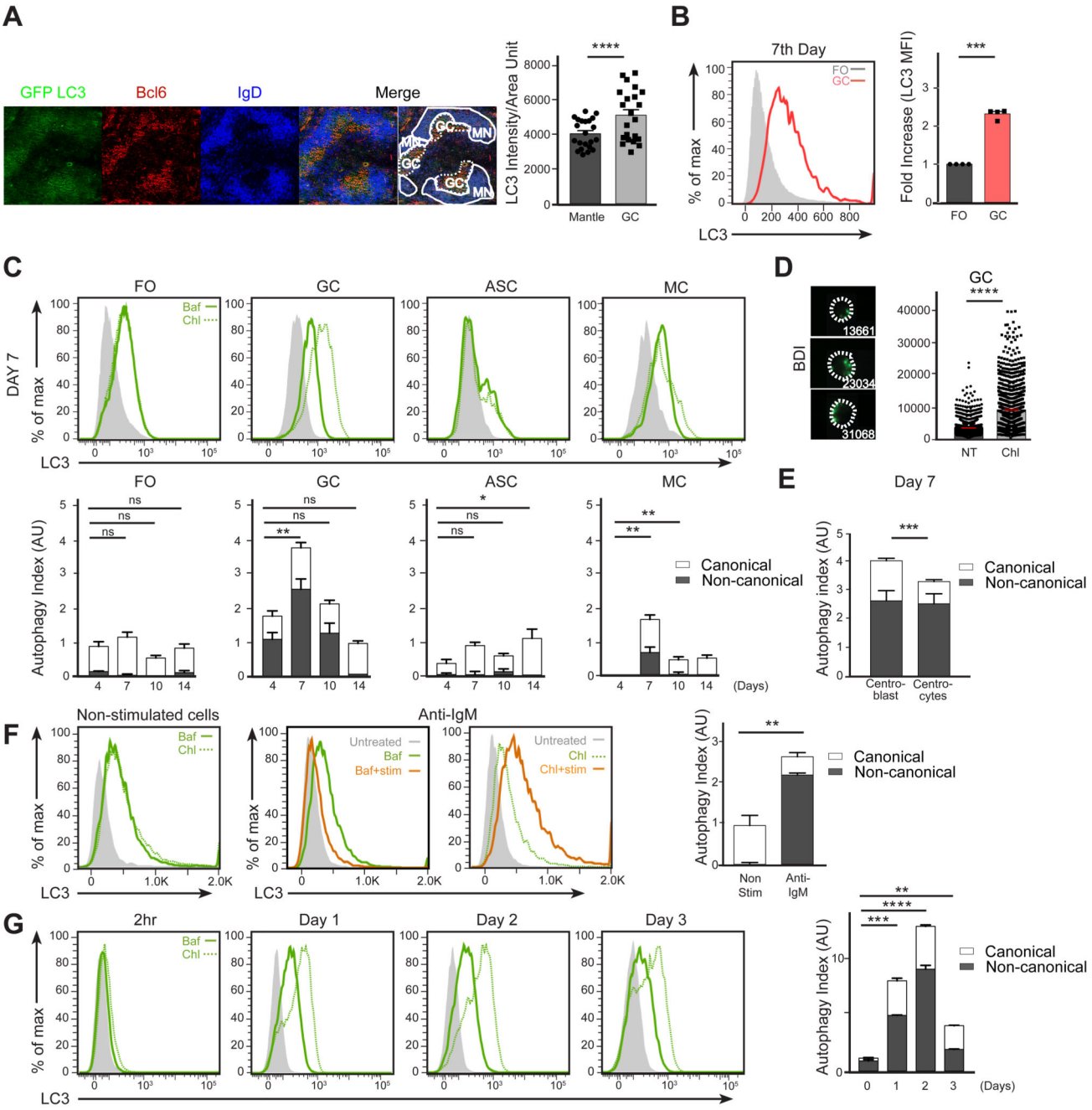

Fig. 1. LC3-II is accumulated in Germinal Center (GC) B cells after viral infection and in naïve B cells after in vitro stimulation.

Results are representative of at least 3 independent experiments. **(A, B, C, D and E)** GFP-LC3 transgenic mice infected with MuHV-4 virus. **(A)** Immunofluorescence of splenic cryosections after 7 days infection showing GFP-LC3 (green), Bcl6 (red), and IgD (blue) Bar charts shows GFP MFI per unit area from GC and mantle (MN). Circles and squares represent individual GC areas. Error bars indicate SEM. **(B)** Flow cytometry histogram showing GFP-LC3-II amounts in GC and Follicular (FO) B cells,. Bar chart shows fold

Europe PMC Funders Author Manuscripts

increase in MFI of GFP-LC3-II in GC cells relative to FO B cells, where circles and squares represent individual mice. Error bars indicate SEM. **(C)** Top: GFP-LC3-II flow cytometry histograms from FO B cells ($B220^{+}CD21^{hi}CD23^{+}$), GC B cells ($CD19^{+}CD95^{+}GL7^{+}$), ASC ($CD19^{+}IgD^{-}CD138^{+}$) and Memory Cells (MC-IgM-IgD^{-}CD138-$B220^{+}IgG^{+}CD38^{+}$) treated with chloroquine (Chl, green dotted line) or BafA1 (Baf, green solid line) or left untreated (grey fill). Bottom: Bar charts showing AI in different B cell types after infection (5 independent mice per day). AU, arbitrary units; error bars indicate SEM. **(D)** ImageStream analysis of GC B cells from splenocytes of virus-infected mice treated with Chl or not treated (NT). Bar chart shows bright detail intensity analysis (BDI) of GFP-LC3-II spots inside the cells (white dotted line). **(E)** Quantification of AI in centrocytes ($CD19^{+}CD95^{+}GL7^{+}CXCR4^{low}CD86^{hi}$) and centroblasts ($CD19^{+}CD95^{+}GL7^{+}CXCR4^{low}CD86^{hi}$). Error bars indicate SEM. **(F)** Flow cytometry histograms (left) from unstimulated naïve B cells treated with Baf (green solid line) or Chl (green dotted line) or left untreated (grey filled) and (right) from IgM-stimulated B cells (orange line) treated with Chl or Baf or left untreated. Bar chart shows quantification of AI. Error bars indicate SEM. **(G)** Flow cytometry histograms of LC3-II accumulation in IgM-stimulated B cells treated with Baf (solid green line) or Chl (dotted green line) or left untreated (grey fill). Bar chart shows quantification of AI. Error bars indicate SEM. *$*P \leq 0.05$; **$P \leq 0.01$; ***$P \leq 0.001$; ****$P \leq 0.0001$; ns, not significant.*

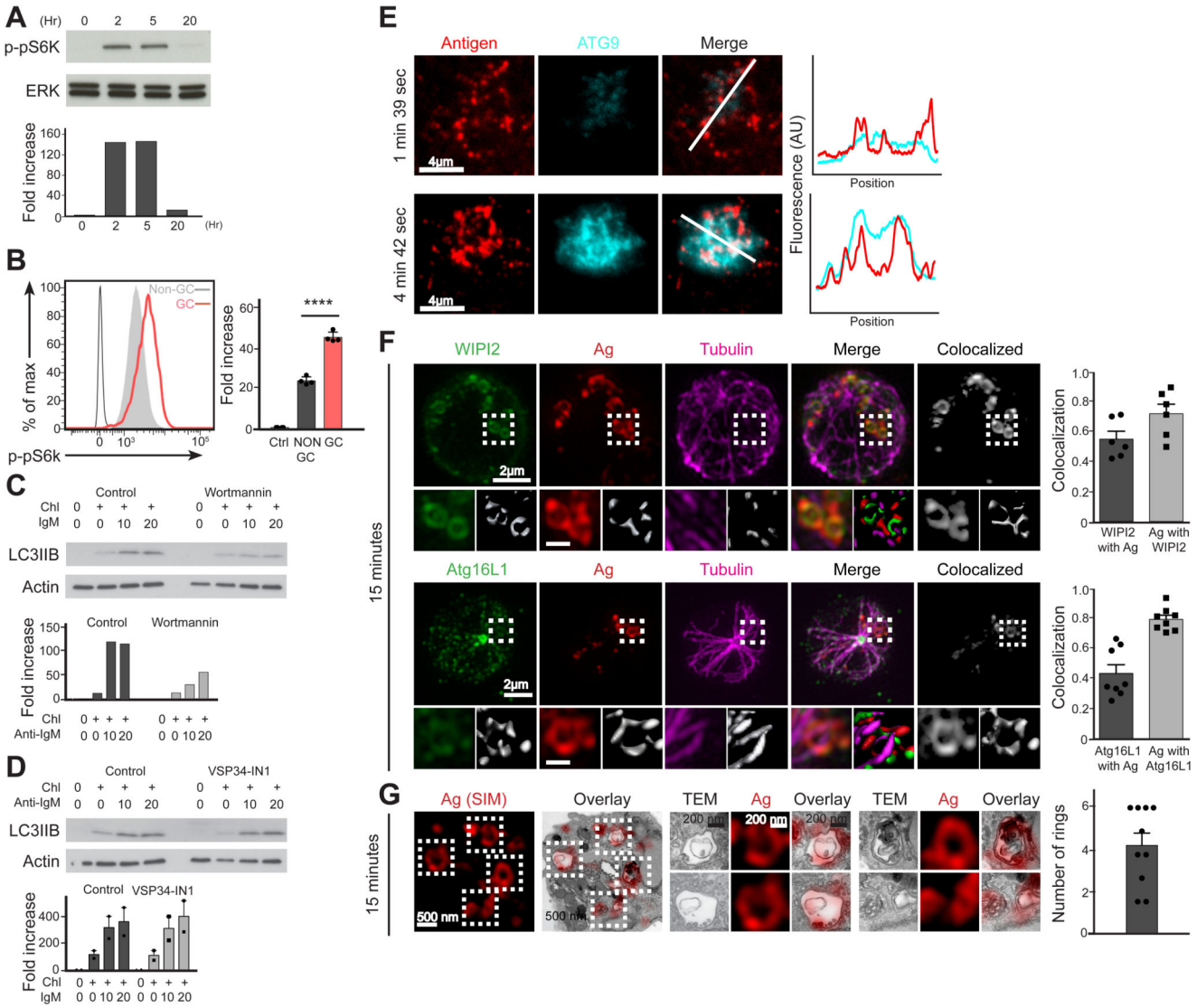

Fig. 2. Autophagy proteins are recruited into antigen-containing rings after BCR internalization.

All data are representative of at least 3 experiments. **(A)** Immunoblot shows mTORC1 activity in naïve B cells after stimulation with CpG and anti-IgM. FBar graph shows fold-increase in phospho-pS6K. ERK, protein control. **(B)** Flow cytometry histogram of p-pS6K in WT GC B cells (red line) and non-GC B cells (gray fill) after MuHV-4 infection (gray line, isotype control). Bar chart shows p-pS6K fold increase. Error bars indicate SEM. **(C and D)** Immunoblots of LC3IIB in WT B cells incubated for 5 hours with or without IgM stimulation (10 or 20 μgl/ml) in the presence or absence of chloroquine (Chl) and wortmannin or VPS34-IN1. Actin, protein control. Bar charts show fold increase of LC3IIB levels relative to unstimulated cells in the absence of Chl. Error bars indicate SEM. **(E)** Left: TIRF microscopy of HEL-specific A20 B cells expressing red fluorescent protein (RFP)-ATG9 on planar lipid bilayer with HEL-Alexa Fluor 633 (a fluorescent dye). Right: Quantification of fluorescent intensities along the white line. Scale bar – 4 μm. **(F)** SIM of WT B cells stimulated in vitro with anti-IgM (Ag. red). WIPI2 or Atg16L1 (green) and

Europe PMC Funders Author Manuscripts

tubulin (magenta) are shown. Bottom subpanels show magnification of three-dimensional surface reconstructions and colocalized images of areas enclosed by the white dashed lines. Scale bar – 2 μm. Bar charts show colocalization (Manders Coefficient) of WIPI2 or Atg16L1 with antigen (Ag).. Error bars indicate SEM. **(G)** Correlative SIM and TEM of ringlike structures in B cells stimulated as in (F) (Scale bar – 500 nm) and magnified images of the areasenclosed by white dashed lines (scale bar – 200 nm). Bar chart shows number of rings per cell. Error bars indicate SEM. ****$P \leq 0.0001$.

Europe PMC Funders Author Manuscripts

Europe PMC Funders Author Manuscripts

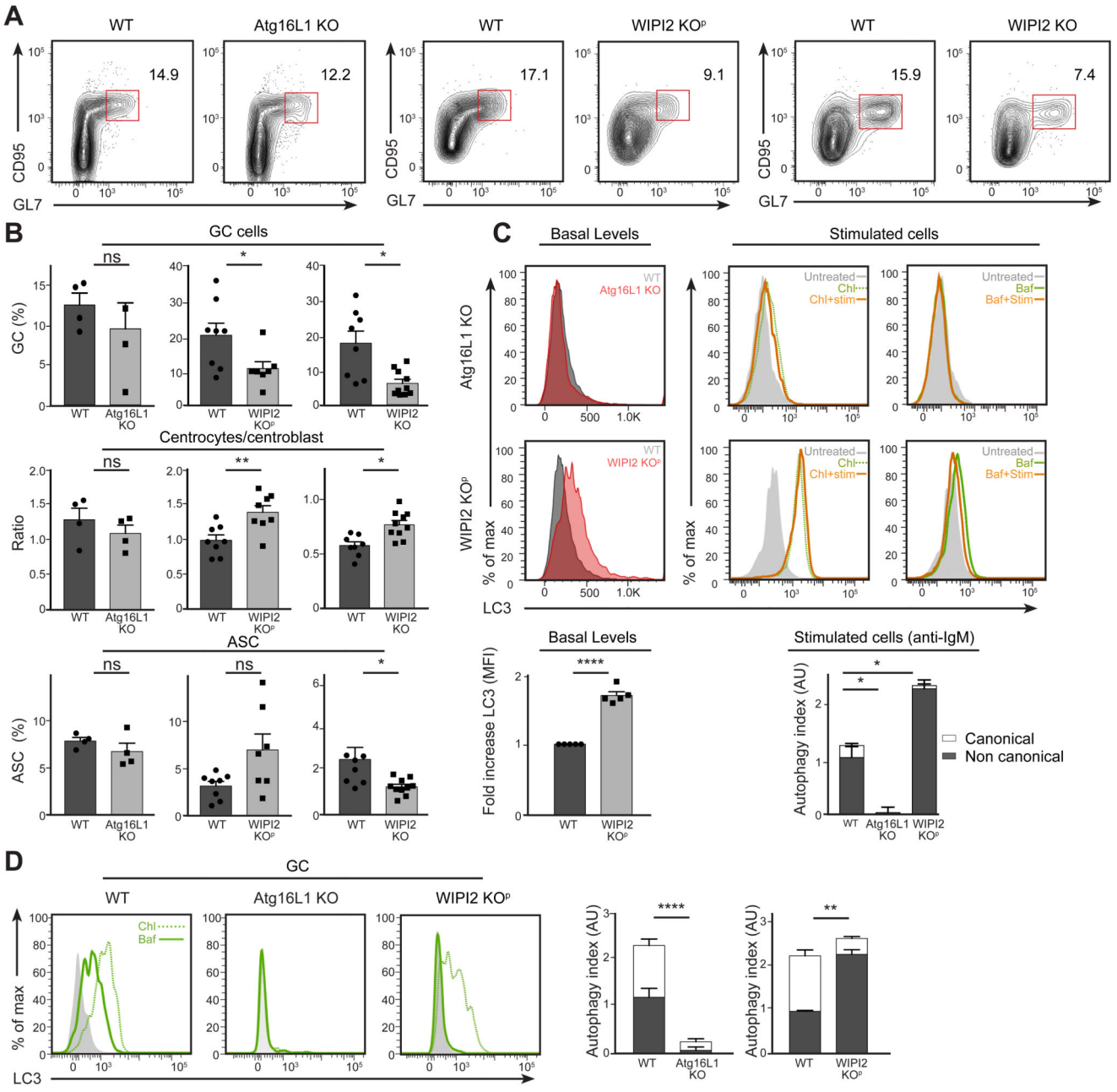

Fig. 3. Noncanonical autophagy is increased in the absence of WIPI2 modifying B cell differentiation.

All data are representative of at least 3 experiments. (**A-B)** Flow cytometry of NP-KLH-immunized WT, Atg16L1-KO and WIPI2-KO^{p} mice (day 13 post-immunisation). (A) Representative contour plots show percentage of GC (red rectangles). (B) Quantification of percentage of NP-specific GC B cells, centrocytes/centroblast ratio, and percentage of ASC in the CD19^{+}NP+ population. Circles and squares respresent individual mice; error bars indicate SEM. **(C)** Flow cytometry histograms of LC3-II in naïve B cells from WT (gray) and Atg16L1-KO and WIPI2-KO^{p} mice (red). Left: LC3-II levels of untreated cells in steady

state. Middle and right: Cells treated with either chloroquine (Chl, green dotted line) or BafA1 (Baf, green solid line) with (orange line) and without IgM stimulation for 5 hours. Gray fill represents untreated controls. Bar charts show (left) fold increase of LC3-II steady state levels without any treatment and (right) AI after stimulation with anti-IgM. Error bars indicate SEM. **(D)** Flow cytometry histograms of LC3 accumulation in GC B cells 13 days after NP-KLH immunization. Splenic B cells were incubated *ex vivo* with Chl (green dotted line), Baf (green solid line) or left untreated as a control (gray fill). Bar charts show quantification of AI. Error bars indicate SEM. *$P \leq 0.05$; **$P \leq 0.01$; ****$P \leq 0.0001$; ns, not significant.

Europe PMC Funders Author Manuscripts

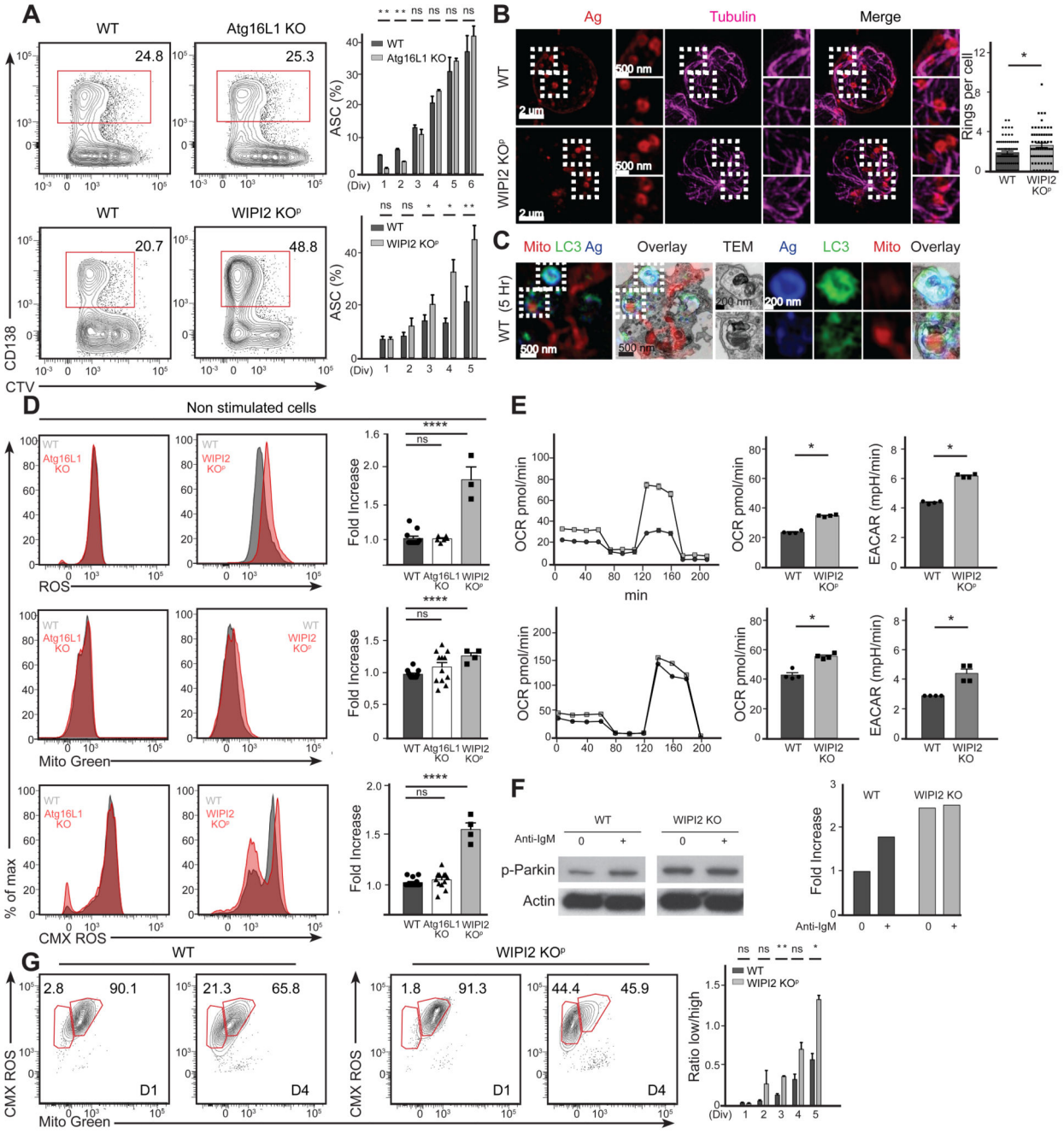

Fig. 4. Metabolic status and mitochondria homeostasis are modified in WIPI2-KO mice.

All data are representative of at least three experiments. **(A)** Flow cytometry contour plots of in vitro ASCs (CD138^{+}, red rectangles) after CpG stimulation. Bar charts show percentage of ASC in each round of cell division. Error bars indicate SEM. **(B)** SIM of WT and WIPI2-KO^{P} B cells 15 min after stimulation. Antigen rings (anti-IgM (Ag). red) and tubulin (magenta). White dashed lines enclose magnified areas. Scale bars, 2 µm and 500 nm. Bar chart shows number of ringlike structures per cell. Error bars indicate SEM. **(C)** Correlative SIM and TEM of mitochondria (red), LC3 (green) and antigen (anti-IgM (Ag), blue) in B

Europe PMC Funders Author Manuscripts

cells stimulated for 5 hours with anti-IgM, CpG and chloroquine (scale bar, 500 nm) and magnified images of the areas enclosed by white dashed lines (scale bar, 200 nm). **(D)** Flow cytometry of unstimulated naïve B cells. Histograms show reactive oxygen species (ROS), mitochondrial mass (MM, Mito Green fluorescent stain), and mitochondrial membrane potential (MMP, CMXRos fluorescent stain). Atg16L1-KO and WIPI2-KO^{p} cells (red) are overlaid with cells of WT littermates (gray). Bar charts show MFI fold increase relative to WT. Circles, squares and triangles represent individual mice; error bars indicate SEM **(E)** Dot plot show oxygen consumption rate (OCR) measured in WT (black), WIPI2-KO and WIPI2-KO^{p} (gray) unstimulated naïve B cells. Bar charts show total OCR (pmol/min) and extracellular acidification rate (ECAR, milli-PH units per minute (mpH/min)). Error bars indicate SEM. **(F)** PhosphoS65-Parkin immunoblot from WT and WIPI2-KO mice B cells with or without IgM stimulation. Bar chart shows phosphoS65-parkin fold increase. **(G)** Flow Cytometry of B cells stimulated with CpG for 3 days. Contour plots show total MM and MMP at division peaks 1 and 4. Bar chart shows low/high MM-MMP population ratio at each division peak. *$P \leq 0.05$; **$P \leq 0.01$; ****$P \leq 0.0001$; ns, not significant.